Atomic and Nuclear Analytical Methods

H.R. Verma

Atomic and Nuclear Analytical Methods

XRF, Mössbauer, XPS, NAA and Ion-Beam Spectroscopic Techniques

With 128 Figures and 24 Tables

Springer

Prof. Dr. H.R. Verma
Punjabi University
Patiala 147 002, India
E-mail: drhrverma@yahoo.com

Library of Congress Control Number: 2006940685

ISBN-10 3-540-30277-8 Springer Berlin Heidelberg New York
ISBN-13 978-3-540-30277-3 Springer Berlin Heidelberg New York

Springer is a part of Springer Science+Business Media.

springeronline.com

Typesetting by SPi using a Springer LaTeX macro package
Cover design: eStudio Calamar Steinen

Printed on acid-free paper SPIN 10908259 57/3100/SPi 5 4 3 2 1 0

Dedicated

to

the fond memory of

my dear daughter

GAGANDEEP

who was keen to see this book

in print but lost her life

in a road accident

on Aug. 9, 1997

at the young age of

15 years & 10 months

Preface

Generally speaking, the Nuclear Science Laboratories of the universities and other research institutes support infrastructure for the application of atomic and nuclear measurement techniques to a variety of fields. These laboratories have state-of-the-art equipment for detecting and measuring all sources of α-, β-, and γ-radiation and are equipped with a broad range of detection systems for measuring and analyzing nuclear radiation. Semiconductor, scintillation and gas-filled detectors including Ge(Li), Si(Li), and NaI(Tl) are available with the necessary supporting electronics. A variety of standard α-, β-, X-, and γ-radiation sources are available for calibrating (energy and efficiency) these detectors and performing other studies with radiation detectors. To perform data acquisition and analysis, a network of personal computers complete with multichannel analyzer software, is interfaced to computer-controlled nuclear electronics components. These computers are equipped with commercial software for statistical analysis, spectral unfolding and other data analysis. For undertaking the research activities in these laboratories, the Master level and research students are trained in experimental methods in the field of radiation physics.

The term "Research" describes innovation, which means development with existing technology and for the development of existing technology. While basic research is motivated by curiosity, the applied research is designed to be useful for specific needs. The main research activities in the field of low-energy physics are oriented towards atomic and nuclear physics. Applied research in the field is devoted to the development and implementation of Atomic and Nuclear Analytical Methods such as *X-ray fluorescence spectrometry*, *Mössbauer spectrometry*, *X-ray photoelectron spectroscopy*, *Neutron Activation Analysis* and *accelerator-based Ion beam analysis* (IBA) *spectroscopy* in various interdisciplinary studies for qualitative and quantitative analysis of various elements in industrial/biological/metallurgical/geological samples. XRF, Mössbauer spectroscopy, and X-ray photoelectron spectroscopy are the table-top techniques, which make use of the radioactive sources while the ion-beam measurements involve the particle accelerators. By accelerating particles to

different energies and smashing them into targets, different phenomena at both the atomic and the nuclear level have been observed. The ion beam analysis is based on the interaction between accelerated charged particles and the bombarded material leading to the emission of particles or radiation whose energy is characteristic of the elements, which constitute the sample material. The spectrometric analysis of this secondary emission may lead to the detection of specific elements as well as the determination of the concentration of these elements and the determination of the nature, thickness, position, or concentration gradient of several layers of elements or compounds.

It is the proud privilege of the author to be primarily associated in teaching and research relating to many of the analytical techniques. It was a long felt desire to provide the material in a unified and comparative form for the students to fulfill the requirement of the course material for extensive studies as well as for researchers engaged in these fields. Keeping this in mind, a comprehensive write-up of X-ray fluorescence (XRF), Mössbauer spectroscopy (MS), X-ray photoelectron spectroscopy (XPS), neutron activation analysis (NAA), particle-induced X-ray emission analysis (PIXE), Rutherford backscattering analysis (RBS), elastic recoil detection (ERD), nuclear reaction analysis (NRA), particle-induced γ-ray emission analysis (PIGE) and Accelerator Mass Spectrometry (AMS) has been presented in this book. I hope that this attempt will yield fruitful results to its readers.

Acknowledgement

I am thankful to my wife Mrs. Baljit K. Verma for her endurance during the time I was awfully busy in not only writing this book but also throughout my research career. Thanks are also due to my sons Nitinder and Deepinder who gave me the moral support and had to bear the loss of my full company during their pleasurable young days.

I am grateful to all the honorable authors and publishers of various books and journals, the works/publications of whom have been consulted during the preparation of this book and referred therein.

My special thanks are due to Dr. Claus Ascheron Executive Editor Physics (Springer-Verlag) for his keen interest, valuable suggestions and kind cooperation throughout this project − right from manuscript to its publication. Thanks are also due to the learned referee for his systematic evaluation, logical observations and constructive suggestions. The appreciable efforts, made by Ms. Adelheid Duhm and Ms. Elke Sauer (Springer-Verlag) and Mr. K. Venkatasubramanian (SPi, India), in bringing out the book in its present form, are thankfully acknowledged.

Patiala, February 2007 *H.R. Verma*

Contents

1

X-ray Fluorescence (XRF) and Particle-Induced X-ray Emission (PIXE)

1.1 Introduction

X-ray Fluorescence (XRF) and Particle-Induced X-ray Emission (PIXE) are the two well-established nondestructive analytical techniques of X-ray emission spectroscopy. These techniques are powerful tools for rapid multielement nondestructive analyses and enable simultaneous detection of many elements in a solid or liquid with high-detection sensitivities, even in those cases where only small sample amounts are available. The fluoresced X-rays from the sample are collected and displayed with either energy dispersive or wavelength dispersive detector systems. The elements are identified by the wavelengths (qualitative) of the emitted X-rays while the concentrations of the elements present in the sample are determined by the intensity of those X-rays (quantitative). XRF and PIXE have emerged as efficient and powerful analytical tools for major, minor, and trace elemental analysis in a variety of fields like biology, environment, medicine, archaeology, and forensic science. These techniques can be used for analyzing rocks, metals, ceramics, and other materials. Handling of samples is greatly simplified by the open-air nature of the instrument used for XRF studies. However, operation outside a vacuum chamber has the disadvantage of decreased sensitivity to light elements.

XRF and PIXE techniques are similar in their fundamental approach and are based on the common fact that when an electron is ejected from an inner shell of an atom, an electron from a higher shell drops into this lower shell to fill the hole left behind. This results in the emission of an X-ray photon equal in energy to the energy difference between the two shells. However, the difference between the two techniques is the mechanism by which the inner-shell electron is emitted. The major difference between XRF and PIXE lies in the mode of excitation. In the XRF technique, high-energy X-ray photons are directed at the sample and this ejects the inner shell electrons while in the PIXE technique, the inner-shell electrons are ejected when protons or other charged particles, like He-ions, are made to impinge on the sample. The first Born approximation predicts in general that the excitation produced by different

charged particles should depend only on their charge and velocity, provided that the velocity is large compared to that of the electrons of interest in the target atom. If the velocity is high enough, not only should electrons and protons produce the same excitation but it is also the same as that produced by photons. The other differences between XRF and PIXE, such as excitation characteristics (mechanism of inner-shell excitation, effect of heavier projectiles/charge state effect, production of nondiagram lines, etc.), background distribution, analytical volume, lower limits of detection, and types of samples analyzed are also of importance and will also be discussed in this chapter.

The field of XRF is not only active at the international level but the IAEA is interested to extend the applicability range of the XRF technique, is apparent from the latest research paper by Markowicz et al. (2006) who have elaborated the specific philosophy behind the functioning of the IAEA XRF Laboratory at Seibersdorf Austria and its role in the XRF community including the methodological development and construction of XRF instruments in order to extend the applicability range of the XRF technique, particularly in support of applications of the analytical technique in developing IAEA member states.

1.2 Principle of XRF and PIXE Techniques

The principle of both of these techniques is to excite the atoms of the substance to be analyzed by bombarding the sample with sufficiently energetic X-rays/γ-rays or charged particles. The ionization (photoionization for XRF and ionization caused due to Coulomb-interaction in case of PIXE) of inner-shell electrons is produced by the photons and charged particles, respectively. When this interaction removes an electron from a specimen's atom, frequently an electron from an outer shell (or orbital) occupies the vacancy. The distribution of electrons in the ionized atom is then out of equilibrium and within an extremely short time ($\sim 10^{-15}\, s$) returns to the normal state, by transitions of electrons from outer to inner shells. When an outer-shell electron occupies a vacancy, it must lose a specific amount of energy to occupy the closer shell of more binding energy. This amount is readily predicted by the laws of Quantum Mechanics and usually much of the energy is emitted in the form of X-rays. Each of such electron transfer, for example from the L-shell to the K-shell, represents a loss in the potential energy of the atom. When released as an X-ray photon, the process is X-ray emission. This energy appears as a photon (in this case a Kα photon) whose energy is the difference between the binding energies of the filled outer shell and the vacant inner-shell. In the normal process of emission, an inner-shell electron is ejected producing the photoelectron. Similarly, in the ion–atom collisions one or more of the atomic electrons can get free (single or multiple ionization), one or several electrons can be transferred from one collision partner to the other, one or both of the collision partners can become excited, and a combination of these

elementary processes can also take place. The excess energy is taken away by either photons (characteristic X-rays) – when an electron from a higher level falls into the inner-shell vacancy or Auger (higher-shell) electrons – when the energy released during the process of hole being filled by the outer shell electron, is transferred to another higher-shell electron. These emissions have characteristic energies determined fundamentally by the binding energy of the levels. The fraction of radiative (X-ray) decays is called the fluorescence yield, and is high for deep inner-shells. The de-excitation process leading to the emission of characteristic X-rays and Auger electrons is shown in Fig. 1.1. The Auger effect is most common with low-Z elements.

We have seen earlier that an electron from the K shell (or higher shell, if the energy of the impinging radiation (X-rays/γ-rays) or charged particles is less than the binding energy of the K-shell) is ejected from the atom creating a vacancy in that shell as the projectile pass through the target atom. This vacancy is filled by an electron from the L or M shell. In the process, it emits a characteristic K X-ray unique to this element and in turn, produces a vacancy in the L or M shell. For instance, when exciting the K-shell ($1s_{1/2}$), the hole can be filled from $L_{III}(2p_{3/2})$ or $L_{II}(2p_{1/2})$ subshells, leading to $K\alpha_1$

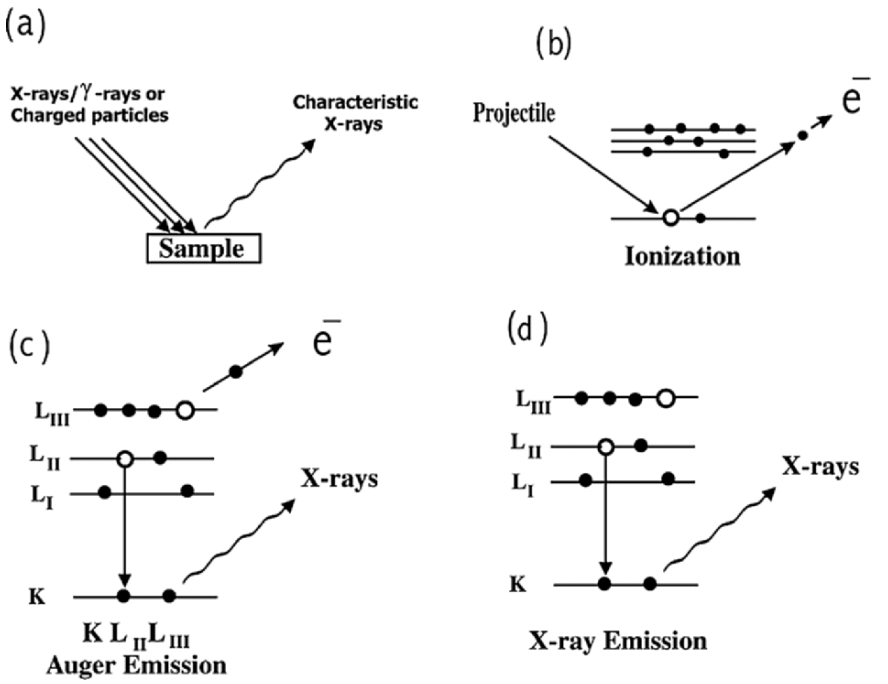

Fig. 1.1. (**a**) Schematic of the phenomenon of X-ray emission (**b**) Vacancy creation in the inner shell by X-rays or charged particles (**c**) process of Auger electron emission comprising of de-excitation and emission of higher-shell electron (**d**) process of X-ray emission

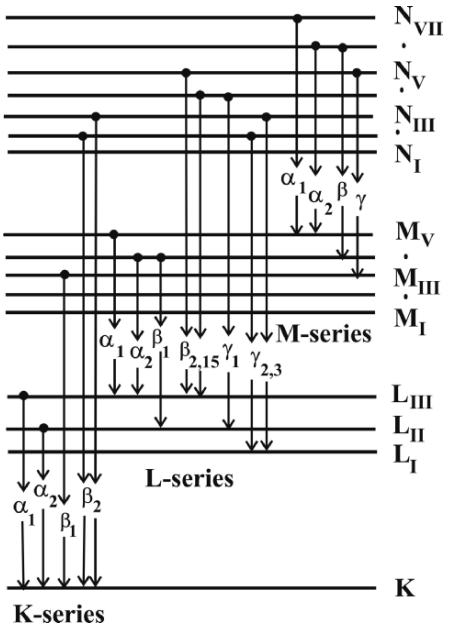

Fig. 1.2. Energy level diagram showing the origin of some of the K, L, and M X-rays

Table 1.1. Designation of various K and L X-ray transitions to denote transitions of electrons

K X-ray Lines	L X-ray Lines	
$K\alpha_1$(K-L_{III})	Ll(L_{III}-M_1)	$L\gamma_1$(L_{II}-N_{IV})
$K\alpha_2$(K-L_{II})	$L\alpha_{1,2}$(L_{III}-$M_{IV,V}$)	$L\gamma_2$(L_I-N_{II})
$K\beta_1$(K-M_{III})	$L\beta_1$(L_{II}-M_{IV})	$L\gamma_3$(L_I-N_{III})
$K\beta_2$(K-$N_{II,III}$)	$L\beta_2$(L_{III}-N_V)	$L\gamma_4$(L_I-O_{III})
$K\beta_3$(K-M_{II})	$L\beta_3$(L_I-M_{III})	$L\gamma_6$(L_{II}-O_{IV})

and $K\alpha_2$ lines. Electrons cannot come from the L_1(i.e. $2s_{1/2}$) sub-shell, because a change in angular momentum is required in the quantum transition. The next shell with electrons is the valence band ($n = 3$) that gives rise to the widely separated and weak Kβ lines. The energy level diagram showing the origin of some of the K, L, and M X-rays is presented in Fig. 1.2.

X-Ray Notation (Siegbahn)

The designation of various K and L X-ray transitions to denote transitions of electrons is given in Table 1.1.

As mentioned earlier, the spectroscopic notation for X-rays will be as:

$$L\alpha_1 \rightarrow 2p_{3/2} - 3d_{5/2}$$
$$L\beta_1 \rightarrow 2p_{1/2} - 3d_{3/2}$$

because the spectroscopic notation for L_I, L_{II}, L_{III}, subshells are $2s_{1/2}$,$2p_{1/2}$, $2p_{3/2}$, respectively, and those for M_I, M_{II}, M_{III}, M_{IV}, and M_V are $3s_{1/2}$, $3p_{1/2}$, $3p_{3/2}$, $3d_{3/2}$, and $3d_{5/2}$, respectively, as explained in Sect. 1.3.

Apart from the characteristic X-ray lines called the diagram lines, non-diagram lines (satellite, hypersatellite and RAE) also appear in the complex K X-ray spectrum. The X-ray lines arising out of the multiply ionized atoms are termed K satellite (KL^n) and K-hypersatellite lines (K^2L^n), where K^mL^n denotes the vacancy from the de-excitation of the double K vacancies and were observed in ion–atom collisions for the first time by Richard et al. (1972). The K satellite lines arise from the group of lines corresponding to the transitions from initial states having one hole in the K-shell and n-holes in the L-shell i.e., $(1s)^{-1}(2p)^{-n} \rightarrow (2p)^{-n-1}$ and represented by $K\alpha L^n$. On the other hand, the hypersatellite X-ray will be due to the $(1s)^{-2} \rightarrow (1s)^{-1}\ (2p)^{-1}$. The double K vacancies are usually filled by the independent transitions of two electrons accompanied by the emission of two photons or Auger electrons. The $K\alpha$ satellite lines will be represented as $K\alpha(2p)^5$, $K\alpha(2p)^4$, $K\alpha(2p)^3, \ldots$ meaning that 5, 4, 3, ... electrons remain intact in the 2p shell while $K\alpha(2p)^6$ will represent the $K\alpha$ principle line with all the six 2p electrons intact. Similar terminology is also used for $K\beta$ satellite lines. Another category in which electron and photon are simultaneously emitted (known as the Radiative Auger effect RAE lines), comprises of single-photon two electron rearrangement transitions (Verma 2000). In the RAE process, the decay of a K-shell vacancy proceeds as a normal K Auger process except that there is emission of a photon along with an electron in addition to an electron filling the K-shell vacancy. Instead of the initial hole being filled with emission of either a full energy $K\alpha$ photon or a full energy Auger electron, there is simultaneous emission of a lower-energy photon $h\nu$ and excitation of an L-shell/M-shell electron, i.e., $h\nu + E_{\rm kin}(Y_j) = E(KY_iY_j)$, where Y denotes an L- or M-shell and i and j denote the concerned subshells. Thus $E_{\rm kin}(Y_j)$ is the kinetic energy of the ejected L_j/M_j-electron and $E(KY_iY_j)$ is the full Auger electron energy. The RAE process competes with the characteristic $K\alpha$ or $K\beta$ X-ray emission processes and produces a broad structure in the X-ray spectra, with energy less than $K\alpha_{1,2}/K\beta_{1,3}$ diagram line.

If the de-excitation takes place during the collision i.e., while the projectile and target electron clouds overlap, "noncharacteristic" molecular orbital (MO) X-ray can be emitted. However, the "characteristic" or separated atom X-rays will be seen if the vacancy de-excites after the collision.

1.3 Theory and Concept

According to the quantum theory, every electron in a given atom moves on in an orbital that is characterized by four quantum numbers:

– *Principal (shell) quantum number* (n) is associated with successive orbitals. The binding energy between the electron and the nucleus is

proportional to $1/n^2$; where n is a positive integer 1, 2, 3, 4, ... that designates the K, L, M, N, ... shells, respectively.
- *Azimuthal (subshell) quantum number* (l) is a measure of the orbital angular momentum which, according to Sommerfeld, accounts for the existence of elliptic and circular electron orbitals; l can take all integral values between 0 and $(n-1)$; $l = 0$ corresponds to a spherical orbital while $l = 1$ corresponds to a polar orbital. A value of $l = 0$ corresponds to s, $l = 1$ is p, $l = 2$ is d, and so forth.
- *Magnetic quantum number* (m) is responsible for determining the shape of an electron's probability cloud (but does not effect the electron's energy) and can take all the integer values between $-l$ to $+l$, including zero. The magnetic quantum number describes the orbitals within a sublevel. Thus for a given value of l, "m" has $(2l+1)$ different values.
- *Spin quantum number* (s) can only take two possible values $+1/2$ and $-1/2$. The spin quantum number, allows two electrons of opposite spin (or symmetry) into each orbital.

The number of orbitals in a shell is the square of the principal quantum number (n) i.e., $1^2 = 1, 2^2 = 4$, and $3^2 = 9$. Furthermore, there is one orbital in an s subshell ($l = 0$), three orbitals in a p subshell ($l = 1$), and five orbitals in a d subshell ($l = 2$). The number of orbitals in a subshell is given by $(2l + 1)$. Since each orbital can accommodate two electrons (one with spin up ($s = +1/2$) and one with spin down ($s = -1/2$) and thus each electron is existing in one of those strange probability clouds, which have widely varying shapes and sizes). The number of electrons in a subshell is given by $2(2l+1)$. Electronic configuration in an energy state is usually designated by symbols containing a number and a letter containing an index, for example $3d^6$. The number "3" represents the principal quantum number while the letters s, p, d, f, g represent the l values 0, 1, 2, 3, 4, respectively. The index number indicates that there are six electrons in this quantum state. This is because of the reason that there are five different shapes for "d" and hence there is room for ten electrons i.e., $2(2l+1)$. The numbers of electrons in any given state are controlled by Pauli's exclusion principle according to which no two electrons can have the identical combination of all the four quantum numbers. The electron configuration (say) for ^{17}Cl is $1s^2\ 2s^2\ 2p^6\ 3s^2\ 3p^5$. The first number represent the energy level, the letters represent the sublevel while the superscripts indicate the number of electrons in the sublevel. The total of the superscripts in an electron configuration equals the atomic number of the element.

The energy levels of different subshells are represented by notation such as $1s_{1/2}$, $2p_{1/2}$, $2p_{3/2}$, ... as shown in Fig. 1.3. States such as $1s_{1/2}$ means $n = 1$, $l = 0$, $j = 1/2$, $2p_{1/2}$ means $n = 2$, $l = 1$ and $j = 1/2$ and $2p_{3/2}$ means $n = 2$, $l = 1$, and $j = 3/2$, where $j = (l \pm s)$. Since the maximum number of electrons in any subshell is given by $(2j+1)$, therefore the number of electrons in $2p_{1/2}$, $2p_{3/2}$ will be 2 and 4, respectively, making a total of 6 electrons in 2p state.

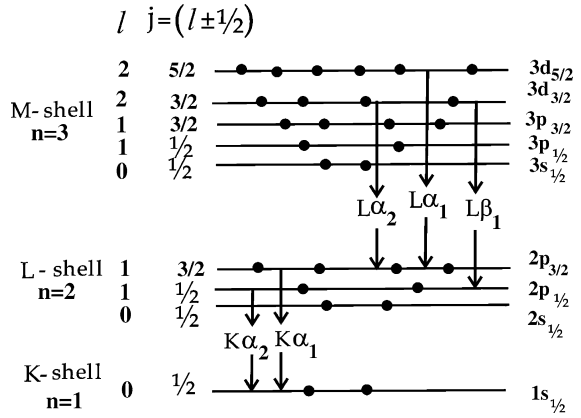

Fig. 1.3. Energy levels of different subshells of an atom along with their quantum numbers and occupancy of electrons

The XRF and PIXE spectra are primarily from transitions that occur after the loss of a $1s$ or $2s$ electron. Transitions that fill in the "$1s$" i.e., K level are of the highest energy, and are called K-lines. Kα_1 and Kα_2 lines are from the $n = 2$ level to $n = 1$ level i.e., Kα_1 originate from $2p_{1/2}$ and Kα_2 from $2p_{3/2}$ and leave a hole in 2p-subshells while Kβ lines leave a hole in the 3p shell. In spectroscopic notation:

$$\mathrm{K}\alpha_1 \rightarrow 1\mathrm{s}_{1/2} - 2\mathrm{p}_{3/2}$$
$$\mathrm{K}\alpha_2 \rightarrow 1\mathrm{s}_{1/2} - 2\mathrm{p}_{1/2}$$

The emission of X-rays is governed by the following selection rules for allowed electric dipole (E1) transitions:

$$\Delta n \geq 1, \Delta l = \pm 1, \Delta j = 0, \pm 1 \tag{1.1}$$

Since the spectroscopic notation for $\mathrm{L_I}$,$\mathrm{L_{II}}$, and $\mathrm{L_{III}}$ are $2s_{1/2}$, $2p_{1/2}$, and $2p_{3/2}$, respectively, while those for $\mathrm{M_I}, \mathrm{M_{II}}$, $\mathrm{M_{III}}$, $\mathrm{M_{IV}}$, and $\mathrm{M_V}$ are $3s_{1/2}$, $3p_{1/2}$, $3p_{3/2}$, $3d_{3/2}$, and $3d_{5/2}$, respectively; the spectroscopic notation for some L X-rays lines is given by

$$\mathrm{L}\alpha_1 \rightarrow 2\mathrm{p}_{3/2} - 3\mathrm{d}_{5/2}$$
$$\mathrm{L}\beta_1 \rightarrow 2\mathrm{p}_{1/2} - 3\mathrm{d}_{3/2}$$

The most important of the forbidden transitions are the magnetic dipole (M1) transitions for which $\Delta l = 0$; $\Delta j = 0$ or ± 1 and the electric quadrupole (E2) transitions for which $\Delta l = 0, \pm 2$; $\Delta j = 0, \pm 1$, or ± 2.

1.3.1 Spectral Series, The Moseley Law

By definition, a spectral series is a group of homologous lines, e.g., the Kα_1 lines or Lα_1 lines, etc. of all the elements. In 1913, Moseley established an

experimental relation between the frequency (ν) of X-rays for each spectral series and the atomic number Z of the element from which it was emitted and expressed it as:

$$\nu = Q(Z - \sigma)^2$$

where Q is the proportionality constant and σ is so-called screening constant. The value of Q is $(3R/4) \times c$ for Kα and $(5R/36) \times c$ for Lα transition. Here c is the velocity of light ($= 3 \times 10^8\,\mathrm{ms}^{-1}$) and R is the Rydberg constant ($= 2\pi^2 me^4/h^3$) which is numerically equal to $1.09737316 \times 10^7\,\mathrm{m}^{-1}$. The energy of different classical circular orbitals is calculated using $E_n = RZ^2h/n^2$ (since $E_n = 2\pi^2 me^4 Z^2/n^2h^2$), where h ($= 4.136 \times 10^{-15}\,\mathrm{eV\,s}^{-1}$) is the Planck's constant. The energies of Kα and Lα X-ray lines can be derived from Bohr's theory will thus be given by:

$$E_{\mathrm{K}\alpha} = (3/4)(Z - \sigma)^2\ E_\mathrm{f}; \quad E_{\mathrm{L}\alpha} = (5/36)(Z - \sigma)^2\ E_\mathrm{f} \tag{1.2}$$

where E_f is the ionization energy of hydrogen atom i.e., 13.6 eV.

The X-ray energies of various Kα and Lα lines increase as a smooth function of the atomic number Z according to the Moseley law $E_x = {Z_\mathrm{eff}}^2 \left(\frac{1}{n^2} - \frac{1}{m^2}\right)$. Here n indicates the lower energy level e.g., 1 for K X-rays, 2 for L X-rays, and so on, while m is the energy level of the higher state e.g., $m = 2, 3, \ldots$ These transitions are energetic enough not to get varied much with oxidation state or chemical bonding of the element. These are therefore used as the fingerprints of various elements to which they belong.

1.3.2 Line Intensities and Fluorescence Yield

The intensity of emission of a particular line (say $\mathrm{L}\alpha_1$ which is $\mathrm{L_{III}}$-$\mathrm{M_V}$ transition) will depend upon various factors, e.g., (a) the probability that the incident radiation will ionize an atom on the $\mathrm{L_{III}}$ level; (b) the probability that the vacant site created on $\mathrm{L_{III}}$ will be filled by an $\mathrm{M_V}$ electron; and (c) the probability that the $\mathrm{L}\alpha_1$ photon will leave the atom without being absorbed within the atom itself (Auger effect).

To calculate the relative intensities of allowed and emitted X-ray lines, we make use of the "sum rule" which states that the total intensity of all lines proceeding from a common initial level or to common final level is proportional to the statistical weight $(2j + 1)$ of that level. For example, the $\mathrm{K}\alpha_2 : \mathrm{K}\alpha_1 = 1 : 2$ (if these are the only electronic transitions proceeding from the $\mathrm{L_{II}}$ i.e., $2\mathrm{p}_{1/2}$ and $\mathrm{L_{III}}$ i.e., $2\mathrm{p}_{3/2}$ subshells) because these transitions are K $\rightarrow$ $\mathrm{L_{II}}$ and K $\rightarrow$ $\mathrm{L_{III}}$, respectively, and the ratio of the line intensities will be the statistical weights of the levels from which the electrons originate i.e., $\mathrm{L_{II}} : \mathrm{L_{III}}$ for which $(2j+1) = 2 : 4$ i.e., $1 : 2$. The intensity ratio $\mathrm{I(K}\alpha_2)/\mathrm{I(K}\alpha_1)$ varies from 0.503 to 0.533 for elements from ${}_{20}$Ca to ${}_{50}$Sn while $\mathrm{I(K}\beta)/\mathrm{I(K}\alpha)$ increases from 0.128 to 0.220 for the above range of elements. The variation in the relative intensities within the L-spectra is more noticeable as given in Table 1.2.

Table 1.2. The variation in the relative intensities of L X-ray transitions

Line →	$L\alpha_1$	$L\alpha_2$	$L\beta_1$	$L\beta_2$	$L\gamma_1$	Ll
Relative Intensity	100	10	50–100	10–20	5–10	3–6

Fluorescence yield is one of the major factors that determine the intensities of X-ray spectra. For each excited state of an isolated atom, the fluorescence yield is defined as $\omega_x = \Gamma_x/\Gamma_{tot}$ in terms of the radiative and total transition probabilities "Γ" for the particular state (the transition probabilities further depend on the angular momentum quantum number, the number of electrons available for transition as well as the excitation energy). The average fluorescence yield is also determined from $\omega_x^{av} = \frac{\sigma_x}{\sigma_x+\sigma_A}$ where σ_x and σ_A represent the X-ray and Auger electron cross-sections, respectively.

Thus the fluorescence yield (ω_K) is related to the number of photons emitted in unit time divided by the number of vacancies formed at that time i.e.,

$$\omega_K = \frac{n\ K\alpha_1 + n\ K\alpha_2 + n\ K\beta + \cdots}{N_K} \tag{1.3}$$

For L- and M-shells comprising of three and five subshells, respectively, if N excited states are produced with population distribution n_i each having fluorescence yield ω_x^i, then the average fluorescence yield for the distribution is given by $\omega_x^{av} = N^{-1}\sum_i n_i\omega_x^i$.

Fluorescence yield values increase with atomic number and also differ significantly from one electron shell to another: ω_K is much larger than ω_L and ω_L is much larger than ω_M. The values of ω_K are known with a higher degree of accuracy than the ω_L values (Bambynek et al. 1972) because the former relate to a one-level shell while the latter are weighted averages for the L_I, L_{II}, and L_{III} shells. Experimental results indicate that ω_K increases from 0.0025 to 0.901 for elements $_6$C to $_{56}$Ba.

1.3.3 Critical Excitation Energies of the Exciting Radiation/Particles

For analysis by XRF technique, the energy of the exciting radiation should be more than the binding energy of the particular shell/subshell (from which the electron has to be knocked out) so that the electron ejection takes place. For example the energy of the incident photon ($h\nu$) should be greater than the binding energy of the K-shell (E_K), called K absorption edge for Kα and Kβ X-ray emission and should be greater than L_I, L_{II}, or L_{III} for $L\beta_3(L_I\text{-}M_{III})$, $L\beta_1(L_{II}\text{-}M_{IV})$, and $L\alpha_{1,2}(L_{III}\text{-}M_V, M_{IV})$ X-ray emission, respectively.

For analysis by PIXE technique, if the incident projectile of charge "Z_1" and mass "M_1" is moving with velocity "V_1" (and hence energy $E_0 = M_1V_1^2/2$) to eject an inner-shell electron from the target having mass M_2, the energy transferred in a head-on collision is

$$T_m = \frac{4M_1M_2E_0}{(M_1+M_2)^2} \approx \frac{4M_1E_0}{M_2} \tag{1.4}$$

Considering that the ejection of the inner-shell electron occurs because of the energy transfer in the collision, the threshold for causing the vacancy due to electron ejection will occur when $T_m = E_K$ (K-shell B.E). Hence $E_0 = (M_2/4M_1) \times E_K = U \times E_K$ where $U = M_2/4M_1$. The experimental results indicate that X-rays are produced at values of U considerably less than this, which indicates that the ionization occurs not by collision with a free electron but by collision with the atom as a whole. Under these circumstances, considerably greater amount of energy can be transferred since the projectile energy is required to be more than the energy of the emitted X-ray for reasons of energy conservation. Since the beam energy is always higher than the limiting value of ∼100 keV), one can safely say that there is no threshold for X-ray production exists in PIXE analysis. There is a threshold of course, which is related to the molecular overlap of orbitals between the individual atoms (target and incident particle) and the compound atom (target plus incident particle). Merzbacher and Lewis (1958) have set a lower limit of 100 keV for incident particle energy, which allows the inequality $\frac{1}{4\pi\varepsilon_0} \times \frac{ze^2}{hv} \ll 1$ to apply.

In the process of X-ray production by electron bombardment however, the electron energy (product of electron charge e and accelerating potential V) must be greater than the binding energy of the shell (i.e., E_K for K X-rays).

The basic concepts regarding ion-energy, ion-current, relative ion velocity, atomic sizes and orbital electron velocities, energy transferred to electrons is discussed in the subsequent sections.

Ion-Energy and Ion-Current

The ion energy depends on the type of accelerator, whether it is single ended or tandem-type. For a single-ended accelerator, $E = qV$ i.e., for 3 MV acceleration voltage, protons will have energy of 3 MeV while Cl^{10+} ions will have energy of 30 MeV. For the Tandem accelerator with accelerating potential of "V" MV where we start with the singly charged negative ions from the source, the energy of the ion beam $E = (q+1)V$.

Since the ion current $I = qe/t$, therefore the ion currents (number of ions/s) $N/t = I/qe$ will be 6×10^6 for 1 pA and 6×10^4 for 100 pA of proton and deuteron beam having $q = 1$. For still heavier ions, the q value will be equal to the charge state of the ions produced in the ion-source due to stripping in the C-foil or Ar-gas. For example for $^4He^{1+}$ and α-particle ($^4He^{2+}$), the charge state (q) values are 1 and 2, respectively. Similarly for $^{12}C^{q+}$, the charge state can have any value between 1 and 6 depending on the number of electrons present on the C-ion. In this case, since the atomic number (Z) of carbon atom is equal to 6, the q-value will be equal to $1, 2, 3, \ldots, 6$ if number of intact electrons on the C-ion are $5, 4, 3, \ldots, 0$ and so on.

Relative Ion Velocities

Since the ion velocity $V_1 = 1.384 \times 10^9 \sqrt{(E_0/M_1)}\text{cm s}^{-1}$

Therefore $(V_1/c) = 0.046 \times \sqrt{(E_0/M_1)}$, where E_0 is in MeV and M_1 is in amu

Thus Relative velocity of 1 MeV protons = 4.6% of velocity of light

Relative velocity of 4 MeV protons = 9.2% of velocity of light

Similarly

Relative velocity of 2 MeV deuterons = 4.6% of velocity of light

Relative velocity of 8 MeV deuterons = 9.2% of velocity of light and

Relative velocity of 4 MeV α-particles = 4.6% of velocity of light

Relative velocity of 16 MeV α-particles = 9.2% of velocity of light

Atomic Sizes and Orbital Electron Velocities

Shell radius $(a_n) = 0.53(n^2/Z)$

Relative velocities of atomic electrons $(v_e/c) = Z/(137n)$, where n is the principal quantum number.

For $_{13}$Al K shell $(v_e/c) = 9.5\%$, for $_{20}$Ca K shell $(v_e/c) = 14.6\%$ and for $_{30}$Zn K-shell electrons $(v_e/c) = 21.9\%$

For $_{82}$Pb K shell $(v_e/c) = 59.8\%$, Pb L shell $(v_e/c) = 29.9\%$ and Pb M shell $(v_e/c) = 20\%$

Maximum cross-sections corresponding to velocity matching demands that the ion velocities from accelerators be comparable with bound electron velocities.

Energy Transferred to Electrons

Since the proton energy $E_p = 0.5\, m_p v_p^2$, therefore for protons energy of 1 MeV, energy transferred to electrons $T = 0.5\, m_e v_e^2$ comes out to be just 11 keV due to ratios of masses of electrons and the velocities of electrons and protons.

Why Particle Energy in the Range of 1–4 MeV u^{-1}?

For Protons

We know that E_p should be less than the Coulomb barrier (E_C) is given by:

$$E_C = \frac{Z_1 Z_2}{\left({M_1}^{1/3} + {M_2}^{1/3}\right)}\text{MeV} \tag{1.5}$$

The velocity matching consideration demand that the maximum ionization cross-sections occur around ion energy (MeV u^{-1}) given by:

$$E_p = 134 U^2 n^4 / Z_2^2 \tag{1.6}$$

For K-shell ionization of $_{15}\text{P}(U = 2.1\,\text{keV}) \Rightarrow E_p = 2.4\,\text{MeV u}^{-1}$

For K-shell ionization of $_{20}\text{Ca}(U = 3.7\,\text{keV}) \Rightarrow E_p = 4.6\,\text{MeV u}^{-1}$

For Deuterons and α-Particles

With heavy ions, the value of ionization cross-section σ_K, σ_{Li} can be calculated from the corresponding proton values using the Z_1^2 scaling law, e.g.,

$$\sigma_{Li}^{ion}(E) = Z_1^2 R \sigma_{Li}^{ion}(E_1/M_1)$$

Thus

$$\sigma_D(E) = \sigma_p(E/2) \text{ i.e. } 2\,\text{MeV protons} \Rightarrow 4\,\text{MeV deuterons}$$
$$\sigma_{He}(E) = 4\sigma_p(E/4) \text{ i.e. } 2\,\text{MeV protons} \Rightarrow 8\,\text{MeV } \alpha\text{-particles}$$

1.4 Instrumentation/Experimentation

1.4.1 Modes of Excitation for XRF Analysis

X-ray fluorescence spectroscopy can be accomplished using (a) radioactive sources as exciters or (b) X-ray tube as exciter.

Radioactive Sources as Exciters

A radioactive source (preferably monochromatic) can be used as an exciter. The sources of ^{55}Fe, ^{109}Cd and ^{241}Am of a few milliCurie (mCi) activity are used as primary sources. The half-life, X-ray/γ-ray energies and analysis range of elements are listed in Table 1.3. For more energies however, the secondary exciters using Cu (8.14 keV), Se (11.37 keV), Y (15.2 keV), Mo (17.8 keV), Sn (25.8 keV), Sm (41.0 keV), and Dy (46.9 keV) can be used with Am^{241} as a primary source. X-rays from the primary source are directed at a selectable secondary exciter target, usually Tin (Sn). The

Table 1.3. Various radioisotopes used as excitation sources

Isotope	Half-life	Energy (keV)	Analysis Range
^{55}Fe[a]	2.7 yr.	5.9, 6.4	Al to Cr for K X-rays
^{109}Cd[b]	470 days	22.16, 24.94 88.03 (γ)	Ti to Ru K X-rays Ta to U for L X-rays
^{241}Am	433 yr.	59.6	Fe to Tm for K X-rays Ta to U for L X-rays

[a] ^{55}Fe decays through EC (100%) to the ground state of ^{55}Mn. The excitation X-rays are the lines from ^{55}Mn.
[b] ^{109}Cd decays to the 88 keV excited state of ^{109}Ag through EC(100%) which further decays to the ground state of ^{109}Ag through γ-ray emission. Thus, the excitation line is the 88.03 keV γ-transition from ^{109}Ag. Using 88 keV γ-transition of ^{109}Cd, one can excite K X-rays of elements from Ru to Pb. (The 22.16 and 24.94 keV are the Kα and Kβ lines from ^{109}Ag.)

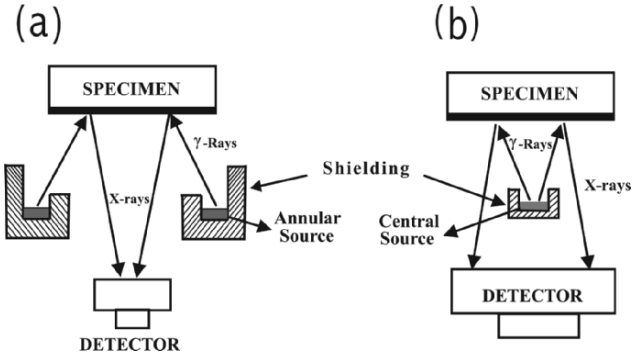

Fig. 1.4. Geometries applied in radioisotope-induced XRF analysis using (**a**) annular source and (**b**) central source

characteristic X-rays from that exciter target are aimed at the unknown sample. This causes emission (fluorescence) of characteristic X-rays from the sample. These X-rays from the sample are captured in a Si(Li) detector and analyzed by computer. The energy spectrum of these X-rays can be used to identify the elements found in the sample.

Typical geometries applied in radioisotope-induced XRF analysis (Lal 1998, Bandhu et al. 2000) using annular and central source are shown in Fig. 1.4a, b. A graded shield of copper and aluminum suppresses low-energy photons in the source. Tungsten alloy collimator with Al lining collimates the photon beam from the secondary X-ray exciters of different metals. A tungsten shield covers the source to avoid direct radiation exposure of the detector. There is a tungsten spacer, which defines the secondary fluorescence target cavity when used in secondary excitation mode and acts as a spacer in the direct excitation mode.

Table 1.3 lists various radioisotopes used as excitation sources for XRF analysis. To perform the qualitative and quantitative XRF analysis based on a radioisotope excitation, one should know the relative intensities and the precise energies of the X- or γ-rays emitted by the source. Verma and Pal (1987) have calculated the K and L X-ray emission intensities for some radio nuclides (^{141}Ce, ^{143}Ce, ^{152}Eu, ^{159}Dy, ^{160}Tb, ^{169}Yb, ^{237}U, and ^{239}Np) using the latest data for γ-ray intensities, electron capture, and internal conversion coefficients for the parent nuclides, fluorescence yield values and Coster-Kronig transition probabilities.

The influence of the photons emitted by a ^{241}Am XRF excitation source below 59.6 keV on sample fluorescence production has been analyzed and general method for evaluating the contribution of the various lines from the source in specific equipment configurations is presented by Delgado et al. (1987). A typical L X-ray spectrum of Pb by ^{241}Am source (Kumar et al. 1999) is presented in Fig. 1.5, which also shows the peaks due to elastically- and inelastically-scattered photons from the ^{241}Am source.

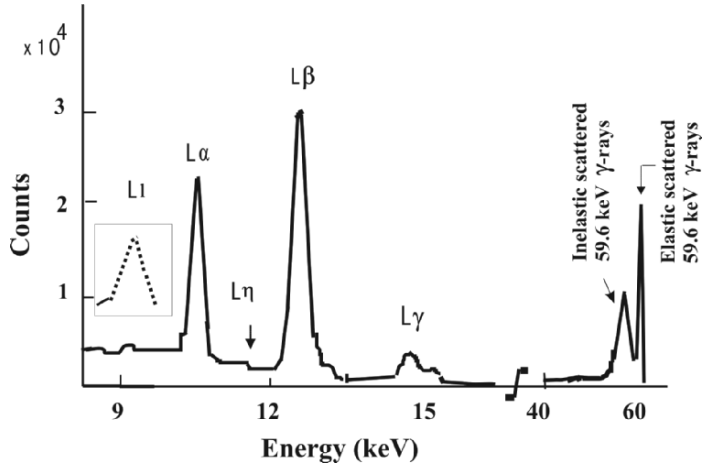

Fig. 1.5. Typical L X-ray spectrum and scattered photons from Pb target by ^{241}Am source

The excitation by X-ray sources requires the knowledge about the values of critical excitation energies of different sources to enable the excitation of inner-shell electrons of various elements present/expected to be present in the sample. Two basic processes i.e., the attenuation and the scattering of X-rays are involved when the intensity is reduced to I_x after the photon beam of intensity I_o passes through the material of thickness x. The reduced intensity is given by Lambert law $I_x = I_o \exp(-\mu x)$, where μ is called the linear attenuation coefficient. The mass attenuation coefficient is further related to the linear attenuation coefficient by $\mu_m = \mu/\rho$ and is the sum of mass photoelectric absorption coefficient (τ) and mass scattering coefficient (σ) expressed in $cm^2\,g^{-1}$. It means that the fraction of intensity $(I_o - I_x)$ that is not transmitted in the same direction as the incident photons is lost mainly as a result of absorption due to photoelectric effect (giving rise to ionization of the atom and emission of X-rays) and the scattering (incoherent/inelastic scattering increasing the wavelength of the incident radiation called Compton scattering or coherent/elastic scattering of unmodified wavelength called Rayleigh scattering). In the low-energy range of photons (<100 keV), the photoelectric absorption coefficient is almost 95% of the attenuation coefficient μ_m. The significant property of the photoelectric absorption coefficient, for any element, is that it increases rapidly with decreases in energy of the photon, falls off vertically at particular value (called the absorption edge) and then again starts increasing again as shown in Fig. 1.6.

The sharp discontinuities in the absorption curve are related to the critical excitation energies (and their corresponding wavelengths) of the element for the K-shell/ L_I, L_{II}, and L_{III} subshells of the L-shell/ M_I, M_{II}, M_{III}, M_{IV}, and M_V subshells of the M-shell, etc. The K- and L-shell absorption edges for a few elements given in wavelength (Å) by Bearden (1967), converted in keV,

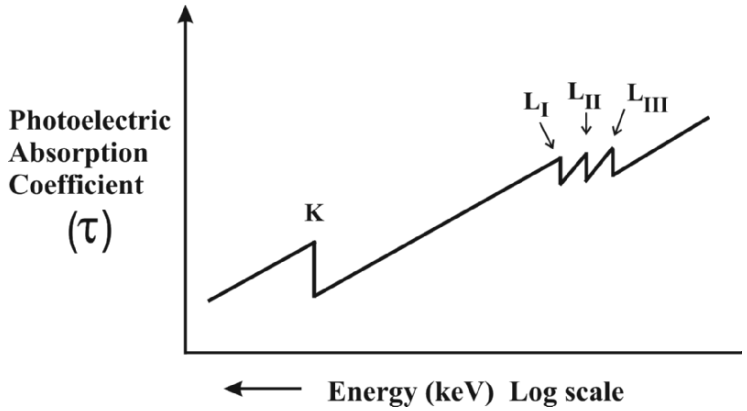

Fig. 1.6. Schematic diagram showing the variation of the photoelectric absorption coefficient as a function of energy for a typical target element

Table 1.4. The K- and L-shell absorption edges for a few elements

Element	Absorption Edge (in keV)			
	K	L_I	L_{II}	L_{III}
$_{11}$Na	1.072			
$_{13}$Al	1.560			
$_{20}$Ca	4.040			
$_{29}$Cu	8.980		0.953	0.933
$_{34}$Se	12.653	1.653	1.475	1.434
$_{39}$Y	17.033	2.377	2.154	2.080
$_{49}$In	27.928	4.238	3.940	3.730
$_{63}$Eu	48.627	8.062	7.621	6.982
$_{73}$Ta	67.391	11.687	11.131	9.880
$_{79}$Au	80.519	14.352	13.732	11.923

are presented in Table 1.4. For example, for $_{73}$Ta, the K absorption edge is at 67.391 keV while the L_{III}, L_{II}, and L_I absorption edges are at 9.880, 11.131, and 11.687 keV, respectively, which means that at 9.880 keV, the critical value for excitation of the L_{III} energy level is reached and ionization at this level is now possible, the sharp increase in absorption that results is called the L_{III} absorption edge. The K absorption edge at 67.391 keV indicates that at energies higher than this, the absorption decreases to very low values.

To detect the X-rays emerging from the sample, a solid state Si(Li) detector, cooled to liquid nitrogen temperature, is used to detect the characteristic X-rays. The detector has a resolution of about 160 eV at 5.9 keV. The pulses from the detector are processed by a shaping amplifier and converted into pulse height by the analog-to-digital converter (ADC) of the multichannel analyzer (MCA).

X-ray Tube as Exciter

X-ray tubes offer greater analytical flexibility at a cost of more complexity. Main features of X-ray tube are as given in Table 1.5.

The considerations for the applied Voltage are as follows:

1. At 50 kV, all K-lines up to $Z = 63$ (Eu) are excited.
2. At 100 kV, all K-lines up to $Z = 87$ (Fr) are excited.
3. 100 kV will excite all K-lines more efficiently than 50 kV, but there are no dispersive crystals available to diffract the lines at a reasonable angle and the background increases so that the line/background remains essentially the same.
4. The intensity of the characteristic X-ray lines of the target of the X-ray tube (overriding the background continuum) are given by $I = A\ C(V - V_{\mathrm{K}})^n$, where A is constant, C is the current, V is the applied voltage which must be equal to the critical voltage V_{K} (in the case of K-lines) and the exponent is a constant that has a value between 1.5 and 2 depending on the emission line. The rapid increase in intensity predicted by the earlier equation does not materialize when V exceeds three or four times the critical voltage V_{K} or V_{L}.
5. The short wavelength limit is given by λ_0 i.e., the spectrum starts abruptly at a wavelength that does not depend on the target material but follows the relation.

$$\lambda_0(\text{in Å}) = \frac{12.39813}{V(\text{in kV})} \tag{1.7}$$

Further, the shorter wavelength limit λ_0 varies as the reciprocal of the applied voltage.

Excitation by the characteristic tube lines may be accomplished by having several different target tubes ($_{24}$Cr, $_{29}$Cu, $_{42}$Mo, $_{45}$Rh, $_{74}$W, $_{78}$Pt or the dual target W/Cr) in any of the desired energy ranges. Mo has advantage for K-lines of $_{32}$Ge to $_{41}$Nb and L-lines from $_{76}$Os and up while Cr is best target for K-lines from $_{23}$V down and L-lines from $_{58}$Ce down. By anode selection, the operator is able to enhance the K lines of Molybdenum ($\sim$17 keV), the L lines of tungsten ($\sim$8 and 10 keV) or the L lines of Molybdenum ($\sim$2.3 keV). By using these lines, especially with a proper filter in between tube and sample, the operator is able to excite fluorescence. Characteristic tube excitation can be used in conjunction with a filter of the target material to reduce the

Table 1.5. Main features of an X-ray Tube

Tube voltage	10–100 kV in steps of 5 kV
Tube current	0–100 mA in steps of 1 mA
Vacuum Pump	Diffusion-Rotary pump
Operating pressure	$\approx 10^{-6}$ Torr
Water flow rate	$\approx$4 litre/min

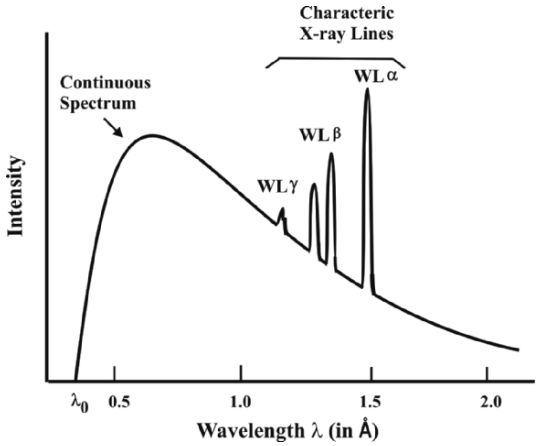

Fig. 1.7. Typical emission spectrum from a $_{74}$W target X-ray tube

background. A typical emission spectrum from a $_{74}$W target X-ray tube is shown in Fig. 1.7.

The continuum or Bremsstrahlung radiation from high atomic number target elements of the tube, which extends to the highest energy of the electron beam, may also be used for excitation. For example the elements up to curium (Kα $\sim$ 40 keV) may be fluoresced using the Bremsstrahlung spectrum and W-target. Both of these give high background. One can find the shortest wavelength λ_0 (highest energy) photon that can be emitted, which corresponds to the incident electron losing all of its kinetic energy in a single collision. For a 35 kV accelerating voltage, the shortest wavelength X-ray that can be emitted is about 0.035 nm. Thus, the continuous part of the X-ray spectrum spans the range from λ_0 to infinitely long wavelengths. The continuous spectrum is used for X-ray diffraction experiments (where X-rays are diffracted by cubic crystals to determine their orientation in space). By changing the target material of the X-ray tube, the effect caused on the continuous X-ray spectrum can be elaborated with reference to Fig. 1.7. The continuous part of the X-ray spectrum varies in intensity with wavelength (equivalent with photon energy $E = hc/\lambda$). There is a broad intensity peak for wavelength near 0.4 Å (0.04 nm), which is somewhat smaller than the spacing of atoms in crystalline solids. The photons with longer wavelengths (lower photon energy) are emitted, although the intensity is not as great as that produced at shorter wavelengths.

Characteristic X-rays are usually used in diffraction experiments where the sample has many different crystal orientations, such as in a polycrystalline or powder sample, as well as for single crystal structure determination. The Kα characteristic line is preferred for use in such experiments since it has the highest intensity. To filter the output of an X-ray tube with the purpose of selecting the prominent line of the target X-ray of the tube, the filter is

chosen with an absorption edge between the two peaks to cause preferential absorption of the peak with shorter wavelength. For example, one mil (0.001″) thick brass foil plus a 1 mil nickel foil can be used over the window of the tungsten X-ray tube. The copper and zinc content in the brass causes high absorption of Lβ and Lγ tungsten lines, while nickel causes high absorption of the Lα tungsten lines.

Wide ranges of X-ray tubes are available with side or end windows. Latest developments in tube technology are the introduction of the dual-anode tubes. In a dual anode tube, a layer of chromium is deposited on a gold substrate or scandium on a molybdenum substrate. At low power the tube behaves like a conventional chromium or scandium tube, but at higher voltages, the radiation from the underlying anode materials is produced to give more excitation of the heavy elements. This enables a single X-ray source to be used over a broad atomic range or in other words excitation can be optimized for general purpose working or for more specialized tasks. The direct optical position sensor (DOPS) goniometer provides remarkable accuracy and reads the θ and 2θ positions from finely etched grating disks which are fitted onto the goniometer axes.

An alternative geometrical set-up known as triaxial geometry (Bandhu et al. 2000) consists of an X-ray tube to fluoresce a selectable secondary target such as Ti, Ag, Ba and to reduce the backscattered radiation is as shown in Fig. 1.8.

The energy of the characteristic X-ray lines produced will be less than the energy of the exciter X-rays. Hence the selection of the target for the X-ray tube is very important. The choice of exciter will depend on the absorption edges of the elements (Table 1.4) present in the sample. Characteristic X-ray production is most efficient when the excitation energy is just above the absorption edge of the particular element of interest. There is a possibility for the variation of voltage (kV) and current (mA) applied to the X-ray tube. The kV and mA settings determine the efficiency with which the X-ray lines are excited in the tube and thus in the sample. The X-ray intensity increases

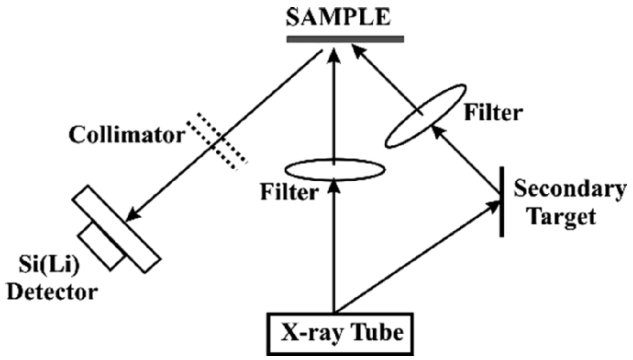

Fig. 1.8. The energy dispersive X-ray fluorescence set-up with triaxial geometry